Updates on numerical implementation and testing of NIMSTELL

Sanket Patil, Carl Sovinec
Department of Engineering Physics
University of Wisconsin-Madison

NIMROD Team Meeting
May 23, 2023.

Work supported by US DOE grants DE-SC0018642 and DE-FG02-99ER54546.

WISCONSIN
UNIVERSITY OF WISCONSIN-MADISON

Outline

- **Motivation and Background**
- 3D Geometry
- Vector potential representation
- Matrix preconditioning developments
- Numerical results

NIMSTELL aims to model non-ideal MHD in 3D configurations.

- Stellarators may allow steady state operation, but it is important to know nonlinear MHD behavior.
- Compared to NIMROD, new capabilities have been implemented:
  - 3D geometry
  - Use of vector potential and *H*(curl) elements
- This presents new challenges with respect to solvers and numerical convergence.

Physical Model: Visco-resistive MHD with fluid closures

$$\frac{\partial n}{\partial t} + \nabla \cdot (n\boldsymbol{V}) = -\nabla \cdot \boldsymbol{\Gamma}_a$$ *Particle continuity with artificial diffusion*

$$mn_i \left(\frac{\partial}{\partial t}\boldsymbol{V} + \boldsymbol{V} \cdot \boldsymbol{V}\right) = \nabla \cdot \left[\frac{1}{\mu_0}\boldsymbol{B}\boldsymbol{B} - \boldsymbol{\Pi} - \left(P + \frac{B^2}{2\mu_0}\right)\mathbf{I}\right] + \boldsymbol{S}_v$$ *Momentum density*

$$\frac{n_i}{(\gamma-1)}\left(\frac{\partial T}{\partial t} + \boldsymbol{V} \cdot \nabla T\right) = -n_i T \nabla \cdot \boldsymbol{V} - \nabla \cdot \boldsymbol{q}_i + S_{Q_i}$$ *Temperature*

$$\boldsymbol{B} = \nabla \times \boldsymbol{A}$$ *Magnetic field-vector potential relation*

$$\frac{\partial}{\partial t}\boldsymbol{A} = \boldsymbol{v} \times \boldsymbol{B} - \eta \nabla \times \nabla \times \boldsymbol{A} - \nabla \chi$$ *Ohm's law*

$$\nabla^2 \chi = C \nabla \cdot \boldsymbol{A}$$ *Gauge condition*

Outline

- Motivation and Background
- **3D Geometry**
- Vector potential representation
- Matrix preconditioning developments
- Numerical results

Finite spectral elements are used for spatial discretization.

- Finite elements tile the poloidal cross-section.
- Elements are rectangular in logical coordinates (ξ, η).
- All fields are represented as polynomials in (ξ, η) of a degree defined by the user.
- Grid points include vertices, internal nodes and edge nodes.

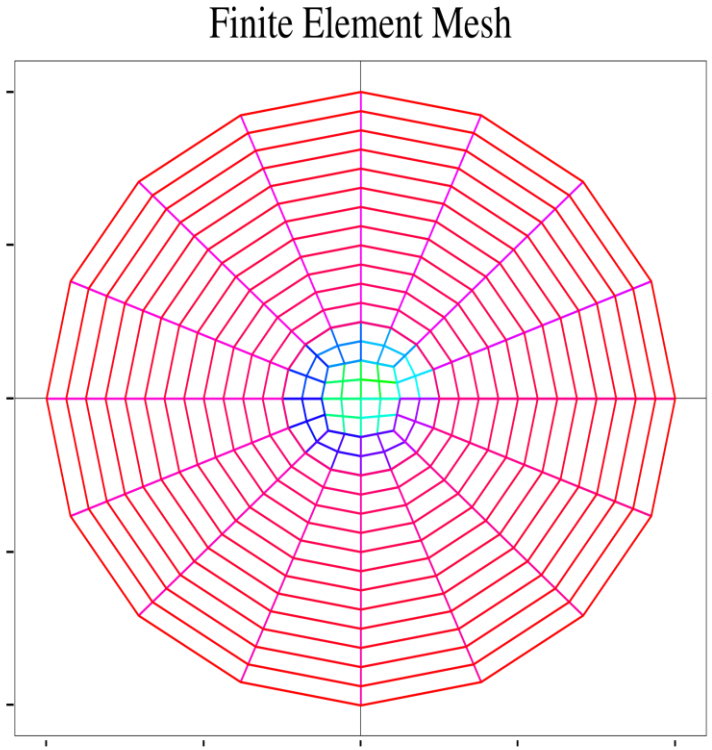

All fields are represented by Fourier series in the toroidal angle.

$$f = f_0 + \sum_{n=1}^{N_{modes}-1} (f_n\, e^{in\zeta} + c.c.)$$

$$f \in \{R, Z, (\phi - \zeta), \boldsymbol{V}, \boldsymbol{A}, n, T\}$$

- 3D geometry is implemented using Fourier series for coordinates (R, Z, ϕ) of FE grid points.
- Generalized toroidal angle may be used:

$$\phi = \zeta + \phi_0 + \sum_{n=1}^{N_{modes}-1} (\phi_n\, e^{in\zeta} + c.c.)$$

- The toroidal grid effectively consists of $N = 2^{lphi}$ poloidal cross sections.
- Dealiasing can be used: $N_{modes} = \frac{2^{lphi}}{n_{dealiase}} + 1$

An interface is used during preprocessing to import 3D equilibria from DESC.

- DESC[1] is used to calculate 3D ideal MHD equilibria.
- DESC uses inverse equilibrium representation $(R(\rho, \vartheta, \zeta), Z(\rho, \vartheta, \zeta))$: generating a flux following grid is straightforward.
- DESC calculates the equilibrium fields at given points in logical coordinates (ρ, ϑ, ζ).
- These values are FFT'd wrt ζ by the interface and read by NIMSET.

[1]Dudt and Kolemen, PoP 27, 102513 (2020)

Outline

- Motivation and Background
- 3D Geometry
- **Vector potential representation**
- Matrix preconditioning developments
- Numerical results

Vector potential is represented in H(curl) basis.

- Nedelec edge elements[2] for the *H*(curl) function space are flexible wrt polynomial degree.

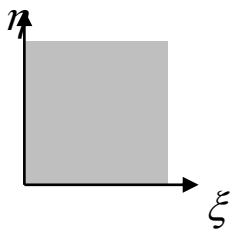

Standard 2D element.

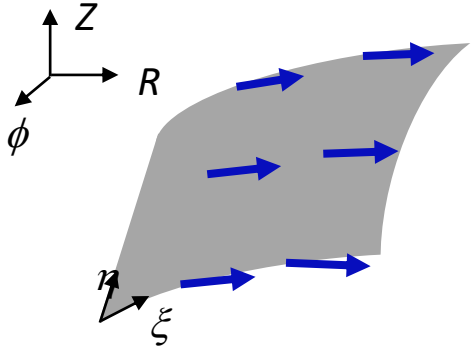

Linear-quadratic nodal $\sigma_k(\xi)\lambda_l(\eta)\nabla\xi$ basis vectors.

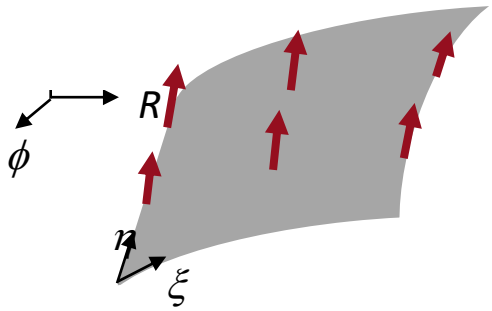

Quadratic-linear nodal $\lambda_k(\xi)\sigma_l(\eta)\nabla\eta$ basis vectors.

- The 1D polynomials $\sigma_k(x)$, $x \in \{\xi, \eta\}$ are for discontinuous expansions.
- The 1D polynomials $\lambda_k(x)$, $x \in \{\xi, \eta\}$ are for continuous expansions and are 1 degree higher.
- The third basis vector is $\lambda_k(\xi)\lambda_l(\eta)\nabla\zeta$.

[2]J. C. Nedelec, Numerische Mathematik **35**, 315 (1980).

Vector potential takes a covariant component form.

- Basis for $\boldsymbol{A}$ is defined separately for each element:

$$\boldsymbol{A} = \sum_{k,l} \left[A_{\xi_{k,l}}(\zeta)\sigma_k(\xi)\lambda_l(\eta)\nabla\xi + A_{\eta_{k,l}}(\zeta)\lambda_k(\xi)\sigma_l(\eta)\nabla\eta + A_{\zeta_{k,l}}(\zeta)\lambda_k(\xi)\lambda_l(\eta)\nabla\zeta \right]$$

- Tangential components are continuous; normal components may not be.
- Divergence constraint $\nabla \cdot \boldsymbol{B} = 0$ within elements follows from $\boldsymbol{B} = \nabla \times \boldsymbol{A}$.

Continuity of $\boldsymbol{B} \cdot \hat{\boldsymbol{n}}$ across element edges is inherent from formulation.

- For example, consider $\hat{\boldsymbol{n}} = \frac{\nabla\xi}{|\nabla\xi|} \propto \frac{\partial \boldsymbol{R}}{\partial\eta} \times \frac{\partial \boldsymbol{R}}{\partial\zeta}$ element surface normals.
- $\frac{\partial \boldsymbol{R}}{\partial\eta}$ and $\frac{\partial \boldsymbol{R}}{\partial\zeta}$ are continuous by construction.

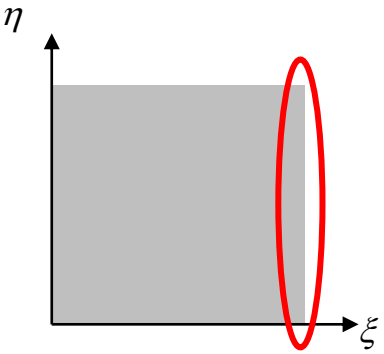

$$\hat{\boldsymbol{n}} \cdot \boldsymbol{\nabla} \times \boldsymbol{A} \propto \frac{\partial \boldsymbol{R}}{\partial\eta} \times \frac{\partial \boldsymbol{R}}{\partial\zeta} \cdot \sum_{k,l} \left[A_{\zeta_{k,l}}(\zeta)\lambda_k(\xi)\lambda_l'(\eta) - \lambda_k(\xi)\sigma_l(\eta)A'_{\eta_{k,l}}(\zeta) \right] \frac{1}{J}\frac{\partial \boldsymbol{R}}{\partial\xi}$$

continuous by Fourier expansion

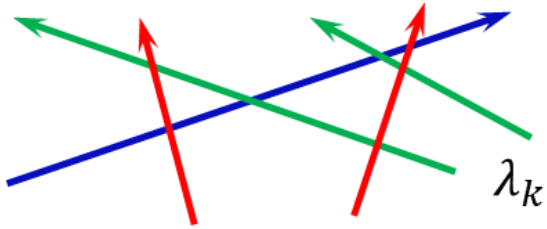

$\lambda_k(\xi) = 0 \; or \; 1$

$\lambda_l'(\eta) \; and \; \sigma_l(\eta)$ are continuous for $0 < \eta < 1$

and $\frac{\partial \boldsymbol{R}}{\partial\eta} \times \frac{\partial \boldsymbol{R}}{\partial\zeta} \cdot \frac{1}{J}\frac{\partial \boldsymbol{R}}{\partial\xi} = 1$

Outline

- Motivation and Background
- 3D Geometry
- Vector potential representation
- **Matrix preconditioning developments**
- Numerical results

A time-step advance requires several linear solves.

- A linear system must be solved for each advance of each of the fields $\boldsymbol{V}, \boldsymbol{A}, n, T$.
- The system of equations is formulated in terms of the Fourier components of the fields.
- Fourier components may be coupled due to 3D geometry.
- The GMRES method is used for iterative linear solves with matrix-free operations.
  - Preconditioner uses formed matrices.

Block-diagonal preconditioning has been developed with bands of modes.

- Iterative methods for solving linear systems converge faster with “preconditioned” matrices.
- Preconditioning is equivalent to multiplication by an approximate inverse of the matrix.
- “Block diagonal” preconditioning uses exact inverses of block-diagonal matrices.
- Using bands of modes with an overlap between consecutive bands has shown promise.

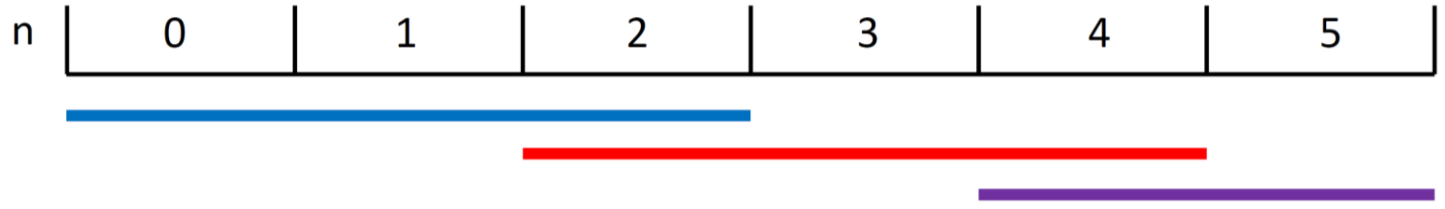

Example set of matrices with *stride* = 2 and *overlap* = 1.

Outline

- Motivation and Background
- 3D Geometry
- Vector potential representation
- Matrix preconditioning developments
- **Numerical results**

Benchmarking against NIMROD for tearing in a circular tokamak is successful.

- Parameters: $R = 10, a = 1, B_0 \sim 1, v_A \sim 1, \nabla p = 0, \eta = 5 \times 10^{-7}, \nu_{iso} = 10^{-10}$.
- $S = 5 \times 10^6, \ Pr_m = 2 \times 10^{-4}$
- Unstable mode: (2, 1)
- The difference in growth rates calculated by NIMROD and NIMSTELL is 0.1%.

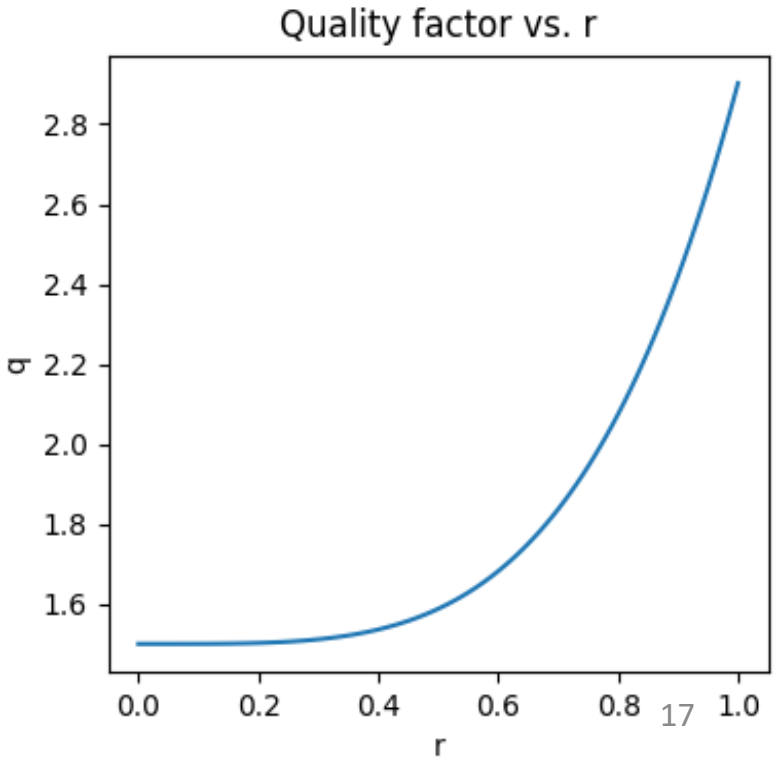

Tearing mode eigenfunctions are localized at the $(2, 1)$ surface.

$\gamma_{NIMROD} = 2.047 \times 10^{-3}\ \tau_A^{-1}$

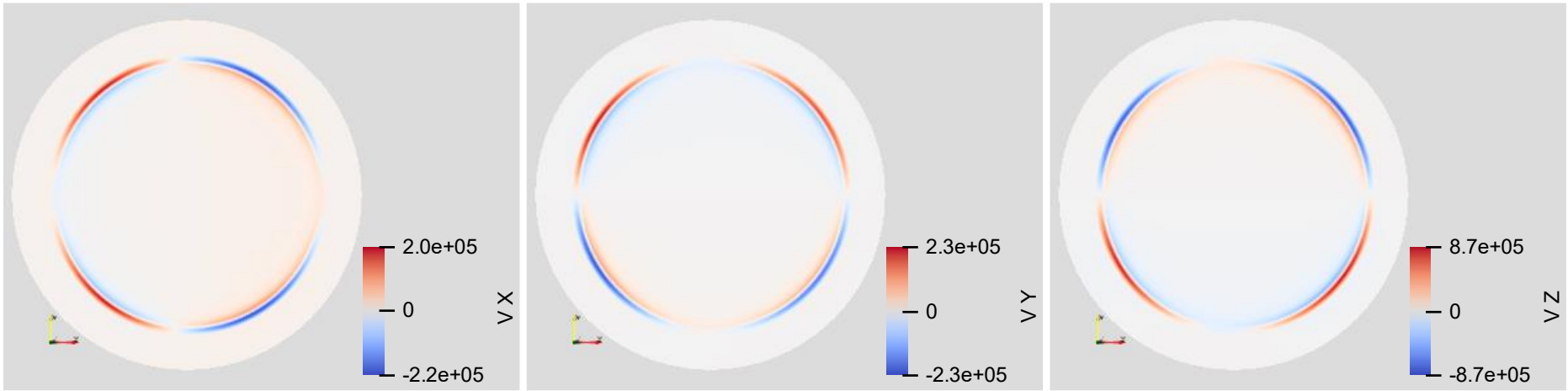

$\gamma_{NIMSTELL} = 2.045 \times 10^{-3}\ \tau_A^{-1}$

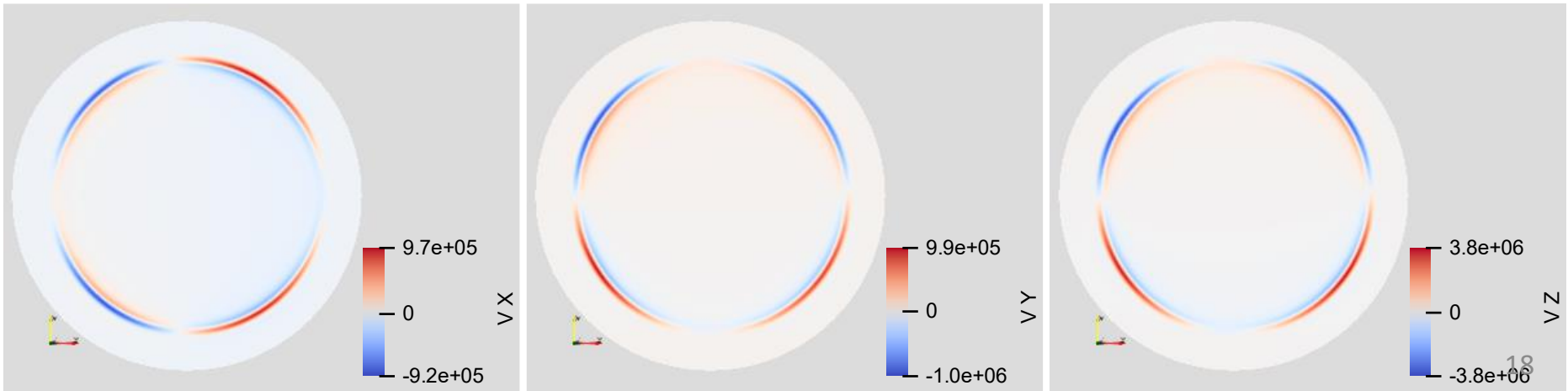

Tearing mode has been obtained in a shaped configuration.

- Shaping: helically rotating elliptical cross section with e = 0.8.
- Magnetic field and boundary shape are helical in the opposite sense: better equilibrium force balance.
- $\eta = 5 \times 10^{-6}, \nu_{iso} = 10^{-8}$
- $S = 5 \times 10^{5},\ Pr_m = 2 \times 10^{-3}$
- Mode shape can be shown through velocity components:

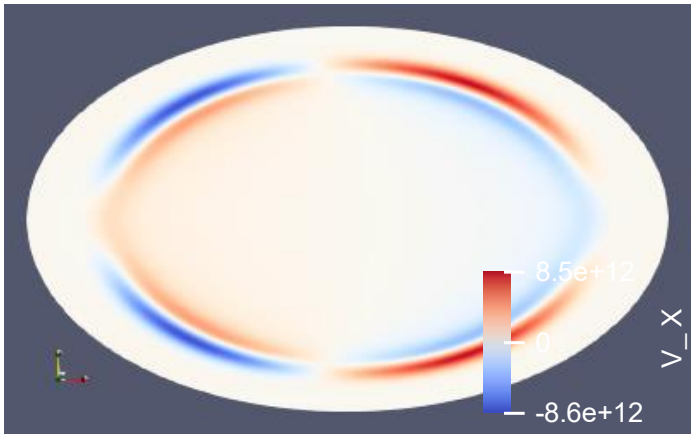

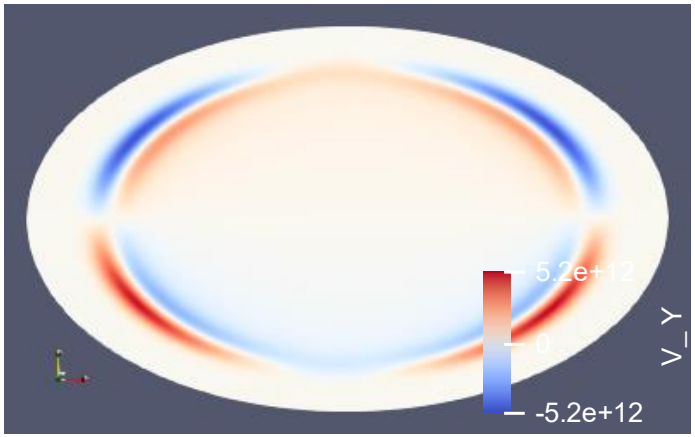

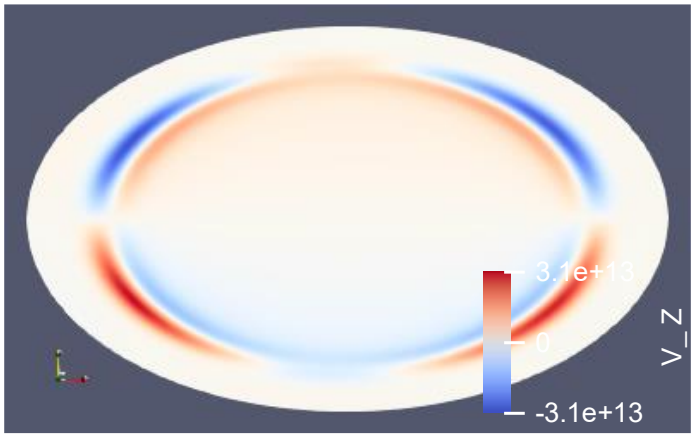

Convergence study for e=0.8 case.

Conv. wrt radial resolution

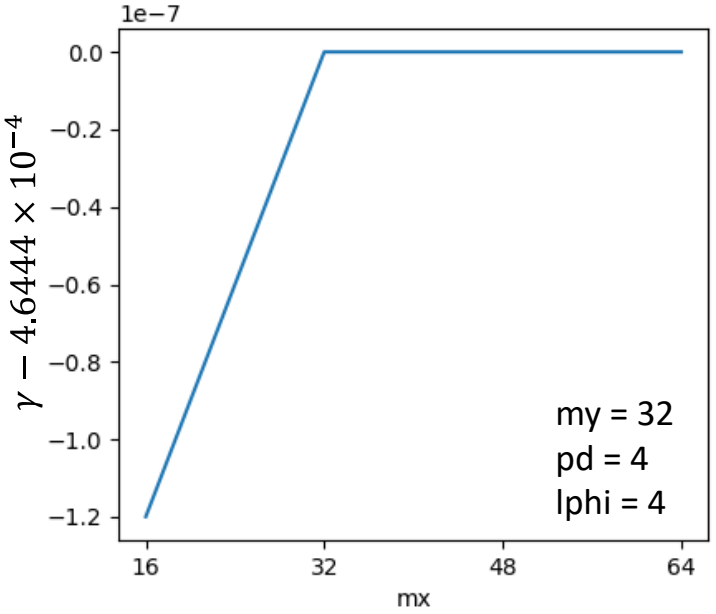

Conv. wrt poloidal resolution

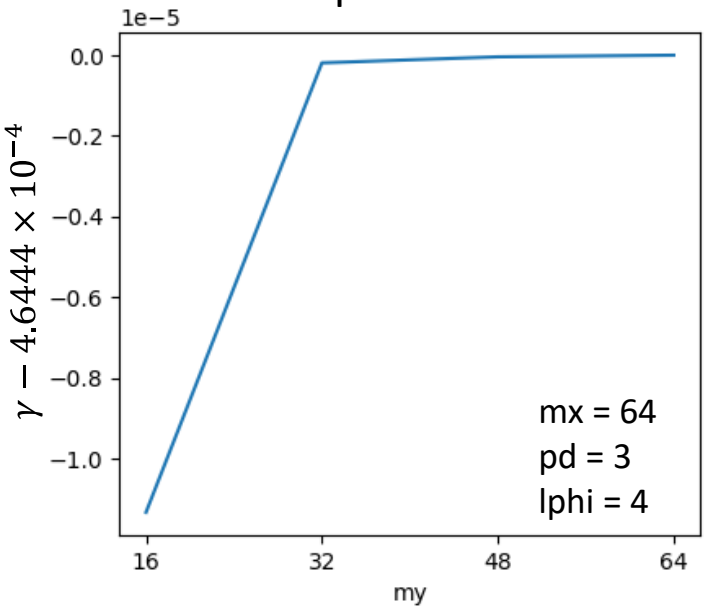

Conv. wrt poly degree

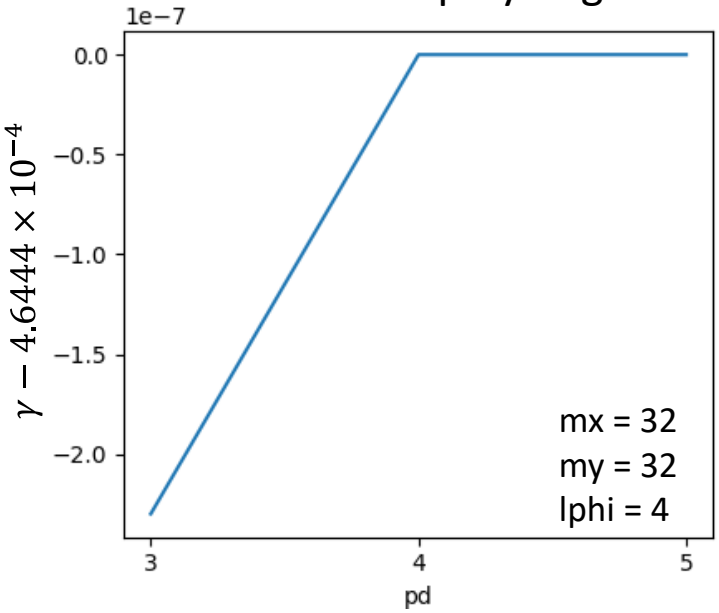

Conv. wrt toroidal resolution

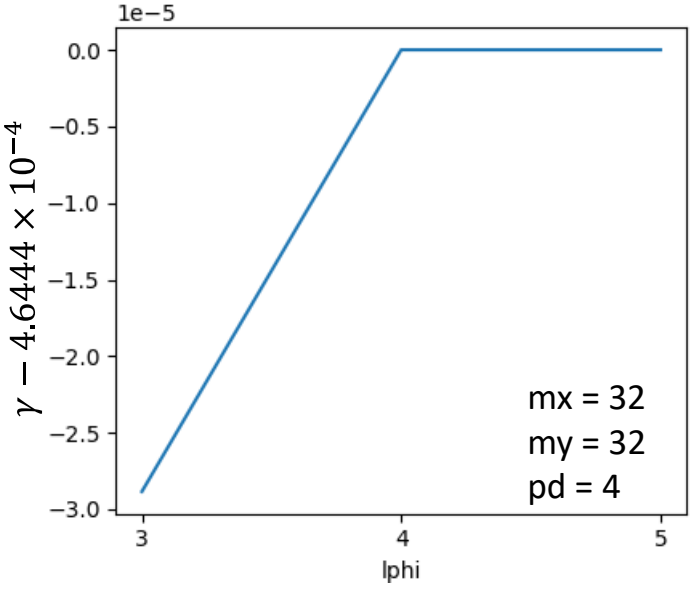

The e = 0.8 case develops numerical instability at lower resistivity ($\eta = 10^{-6}$).

- Numerical instability develops with largest n growing the fastest (contours shown for 48x32, pd=5, lphi=4 grid).
- Higher radial resolutions do not resolve these small features.

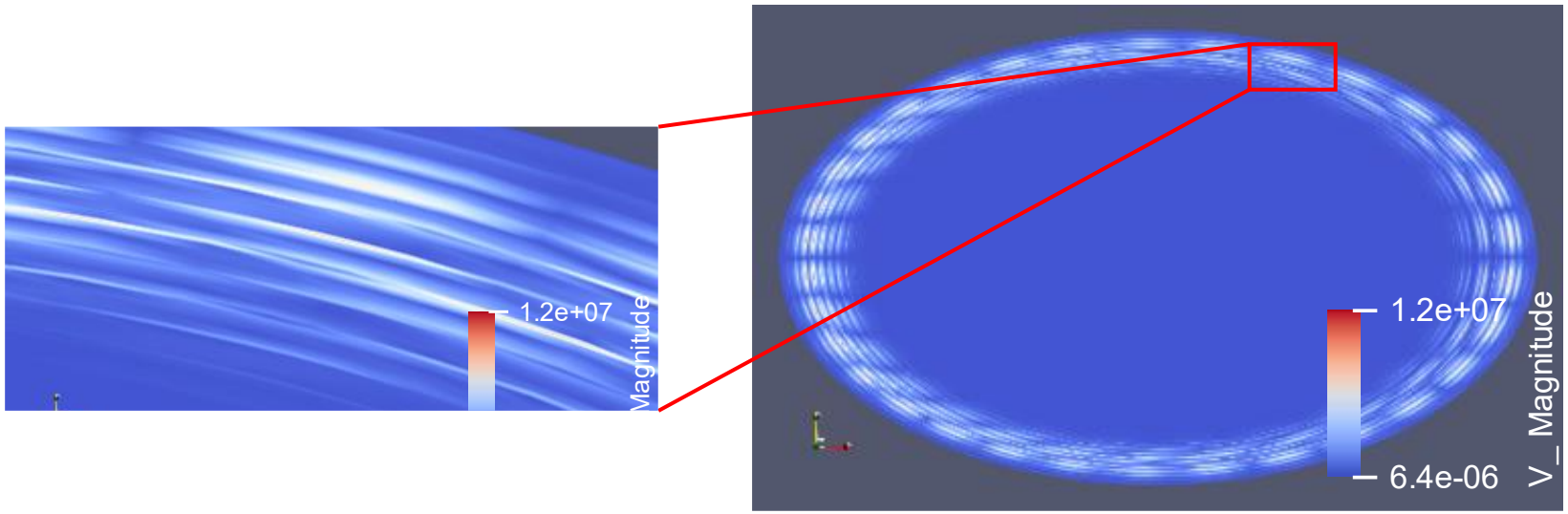

Higher viscosity ($\nu_{iso} = 10^{-7}$) eliminates the features but reveals a different instability.

- Mode with largest n grows the fastest.
- This instability grows faster than the (2, 1) tearing mode.
- Increasing toroidal resolution does not resolve the instability.
- The source of these numerical modes is being investigated.

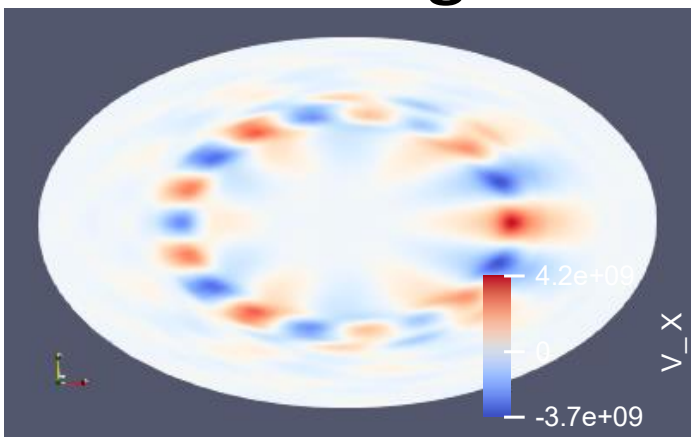

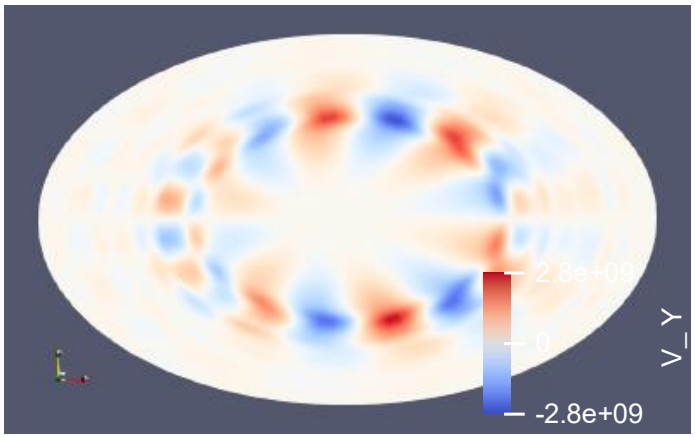

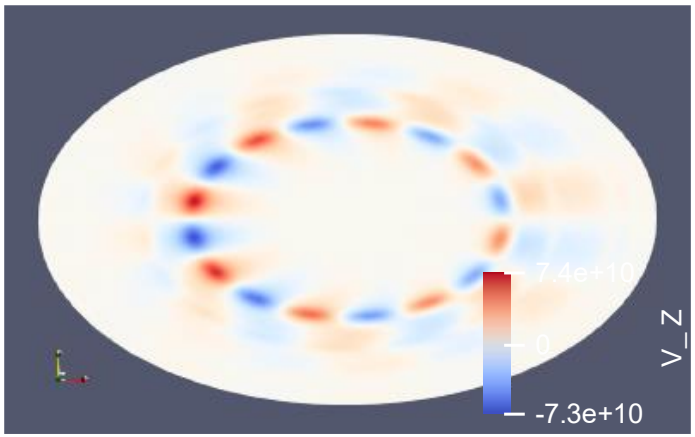

Anisotropic thermal conduction in a quasisymmetric stellarator is successful.

- Configuration: WISTELL-A[3].
- Normalized parameters: $S_Q = 4,\ \chi_{\|} = 6.67 \times 10^5,\ \chi_{iso} = 0.667.$
- Uniform T along boundary, ran to steady state.

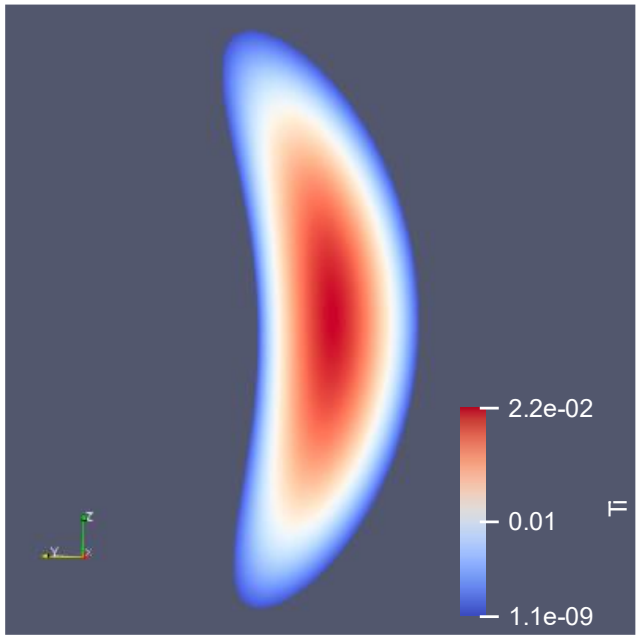

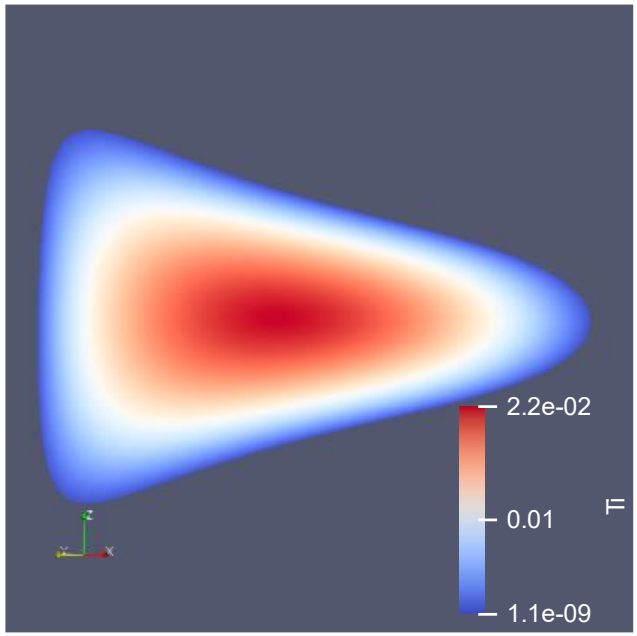

[3]A. Bader, et. al, JPP 86(5), 905860506 (2020).

Future goals

- Analyze the behavior in low resistivity cases.
- Linear stability of other modes, e.g., ballooning.
- Tests with realistic stellarator geometries.
- Use of generalized toroidal angle.
- Nonlinear operators.